Conformational dynamics of a nicotinic receptor neurotransmitter binding site

Mrityunjay Singh[1], Dinesh C. Indurthi[‡2], Lovika Mittal[1], Anthony Auerbach[2‡], and Shailendra Asthana[1‡].

[1]Computational Biophysics and CADD Group, Computational and Mathematical Biology Center, Translational Health Science and Technology Institute, NCR Biotech Science Cluster, Faridabad 121001, India.

[2]Department of Physiology and Biophysics, University at Buffalo, State University of New York, Buffalo, United States.

[‡] Corresponding Author

Shailendra Asthana: sasthana@thsti.res.in

Anthony Auerbach: Anthony.auerbach@gmail.com

Dinesh C. Indurthi: dinesh.indurthi@gmail.com

Key words: acetylcholine, allostery, agonist, induced fit, conformational selection.

Abstract

Agonists activate receptors by interacting more strongly with active versus resting conformations of their target sites. For each ligand, the strong-weak binding free energy difference sets efficacy and the weak/strong ratio sets efficiency. We performed molecular dynamics simulations to explore the conformational dynamics of a nicotinic receptor neurotransmitter binding site in the weak→strong structural transition. The alternative conformations were identified by comparing calculated and experimental binding free energies for 4 agonists. In weak→strong, the agonist rotates about its cationic center (a 'flip'), loop C moves in (a 'flop') to reposition αY190 to form a water-mediated cross-subunit hydrogen bond with the ligand. The flop restructures the aromatic core, and the flip increases van der Waals interactions to generate a more compact, hydrophobic and stable pocket. The simulations reveal a transient intermediate state as well as changes in a salt bridge that may distinguish agonists.

143 words

Introduction

Skeletal muscle nicotinic acetylcholine receptors (AChRs) mediate synaptic transmission between motor neurons and muscle fibers. These pentameric ligand-gated ion channels (pLGICs) are composed of four different subunits (2 α1, β1, δ, and ε) arranged symmetrically around a central ion-conducting pore (Rahman et al., 2020; Unwin, 1993). Binding of the neurotransmitter acetylcholine (ACh) or other agonists to two target sites in the extracellular domain (ECD) increases the probability of a global conformational change that opens a distant (~60Å) channel 'gate' in the transmembrane domain (TMD), to allow water and cations to cross the membrane.

At the start of the channel-opening isomerization the agonist binding sites switch from low to high affinity (LA→HA), and at the end of the isomerization the gate switches from closed to open (C_{LA}→O_{HA}) (Purohit et al., 2013). Without a bound agonist, the probability of the O shape (P_O) is small and baseline activity is negligible (Jackson, 1986; Nayak et al., 2012; Purohit & Auerbach, 2009). Agonists (A) increase P_O because they provide more favorable binding energy to the target in its active vs resting conformation, making O_{HA} more stable than C_{LA}. Agonists also bind strongly to the transition state that separates O from C and so also increase the channel-opening rate constant (Grosman et al., 2000).

The binding free energy difference between high and low affinity (ΔG_{HA}-ΔG_{LA}) drives receptor activation and determines agonist efficacy, the high-concentration limit of the dose-response curve. In contrast, the binding free energy ratio ($\Delta G_{LA}/\Delta G_{LA}$) generates a correlation between the curve's maximum and midpoint and determine agonist efficiency, the fraction binding energy converted into movements that trigger receptor conformational change.

Adult-type muscle AChRs have an unfavorable unliganded isomerization free energy (+8.3 kcal/mol at -100 mV) (Nayak et al., 2012) and 2 approximately equal and independent binding sites a (Nayak & Auerbach, 2017). For ACh, ΔG_{HA}=-10.2 kcal/mol and ΔG_{HA} =-5.1 kcal/mol per site, so adding their differences at 2 sites to that of the intrinsic isomerization, gives -1.9 kcal/mol. A free energy difference is proportional to the logarithm of an equilibrium constant. Hence, after binding 2 neurotransmitters the AChR gating equilibrium constant increases from 7.4×10^{-7} to 25, and P_O increases from ~10^{-6} to 0.96 (Fig. 1A). Binding energy from 2 neurotransmitters turns the receptor approximately from off to on.

Our goal is to associate $\Delta G_{LA} \rightarrow \Delta G_{HA}$ changes with underlying structural rearrangements at the binding site. Here, we use MD simulations to explore the conformational dynamics of the LA→HA transition at the α–δ neurotransmitter binding site of the *Torpedo* AChR (6UVW; (Rahman et al., 2020)). Binding free energies calculated *in silico* aligned with those estimated experimentally by using electrophysiology, so it was possible to interpret the agonist energy changes with restructuring of the binding pocket. It is difficult to draw sweeping conclusions because we examined only 4 agonists and only one wild-type site. However, in the LA→HA transition for all constructs the agonist somersaults, loop C droops to reposition αY190 and rearrange an aromatic pocket that contracts and becomes more hydrophobic. Also, in all systems the initial LA and final HA conformations of the binding site were connected by a brief intermediate state. For some but not all agonists, loop F moves in and a conserved salt bridge shortens. The results suggest that that agonist mobility is important determinant of the increase in binding free energy, and that rather than acting as a lid that closes, loop C is a positioning device that inserts an affinity-increasing side chain into the pocket core.

Results

Hold. Traditionally, receptor activation is divided into binding (formation of a ligand-protein complex) and gating (receptor isomerization). Here, we are concerned only with movements at binding sites that connect these two steps. In binding, the agonist (A) diffuses to interact with the target ($A+C={}^{A}C$), after which a local rearrangement establishes the LA complex (${}^{A}C=AC_{LA}$) (Jadey & Auerbach, 2012). In gating, the site again rearranges to produce the HA complex ($AC_{LA}=AC_{HA}$), after which the rest of the protein domains (ECD, TMD and gate) restructure to establish AO_{HA}. We call the two local rearrangements of the binding site 'catch' (free energy change ΔG_{LA}) and 'hold' ($\Delta G_{HA}-\Delta G_{LA}$) (Fig. 1B). The end of binding is AC_{LA} and the start go gating is AC_{HA}, so hold is the local rearrangement that connects these two activation steps.

The free energy changes associated with the other events in binding and gating, namely diffusion to the site (the chemical potential) and restructuring of receptor domains, are the same for the agonists we have examined and so are not relevant to this study. Furthermore, energy coupling between the binding pocket and distant residues (>15 Å) typically is weak (Gupta et al., 2017) (Fig. S1A). Only catch and hold determine differences between agonists with regard to affinity (ΔG_{LA}, ΔG_{HA}), efficacy ($\Delta G_{HA}-\Delta G_{LA}$) and efficiency ($1-\Delta G_{LA}/\Delta G_{HA}$) (Nayak et al., 2019). In AChRs, ΔG_{LA} and ΔG_{HA} have been measured experimentally for 23 agonists and 53 binding site mutations (Indurthi & Auerbach, 2023) (Fig. S1B). The structures generated in the MD simulations were identified as AC_{LA} or AC_{HA} by aligning ΔG_{LA} and ΔG_{HA} values calculated i*n silico* with those from experiments.

The cryo-EM structures of AChRs include apo, resting-C with a bound toxin and high-affinity desensitized (Rahman et al., 2022; Rahman et al., 2020; Zarkadas et al., 2022). Binding sites of desensitized AChRs have a similar (perhaps identical) high affinity as do O sites (Auerbach, 2020). The end states of the hold rearrangement are short-lived and have not been captured as structures.

Because ΔG_{LA} and ΔG_{HA} are independent of energy changes outside the binding pocket, in the simulations we removed the TMD and studied only $\alpha-\delta$ subunit ECD dimers. The starting structure for the hold transition was (PDB: 6UWZ) after toxin removal that is essentially the same

as the apo structure (Zarkadas et al., 2022)) (Fig. 1C). The 4 agonists we examined were acetylcholine (ACh), carbamylcholine (CCh), epibatidine (Ebt) and epiboxidine (Ebx).

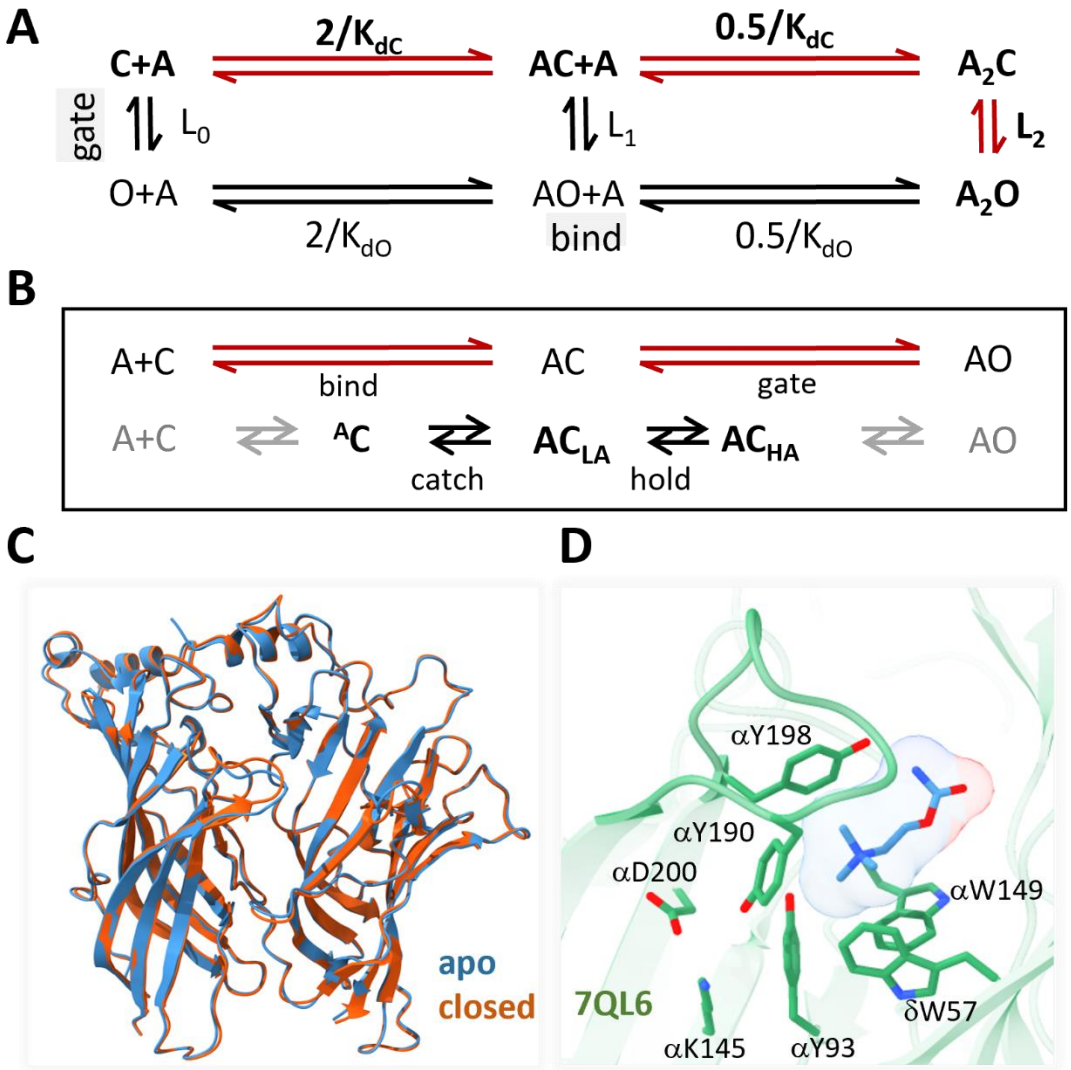

Fig. 1: AChR activation (function and structure). *A.* cyclic activation scheme. Vertical, gating. Receptors isomerize between resting (C) and active (O) conformations (equilibrium constant L_n, where n is the number of bound ligands). Horizontal, binding. Agonists (A) bind weakly to C (equilibrium dissociation constant K_{dC}, free energy change ΔG_{LA}) and strongly to O (K_{dO}, ΔG_{LA}). In adult AChRs the 2 sites are equivalent and independent and there is no significant external energy $L_2/L_0 = (K_{dC}/K_{dO})^2$ (Nayak & Auerbach, 2017). B. intermediate steps in binding and gating. Left, the agonist diffuses to the target to form an encounter complex that then becomes a LA complex by a 'catch' rearrangement. Right, The LA site becomes HA by a 'hold' local rearrangement, followed by domain restructurings that eventually generate a conducting pore. Bold, the. free energy changes in catch and hold (ΔG_{LA} and ΔG_{HA}) determine agonist action. *C.* overlay of α and δ subunits extracellular domains, toxin-less (red, 6UWX.pdb) and apo (blue, 7QKO.pdb). There are no major deviations (C_α RMSD = 0.3 Å). D. α-δ subunit neurotransmitter site with CCh (blue) in a HA, desensitized conformation (7QL6.pdb; (Zarkadas et al., 2022)). The agonist is in the *trans* orientation (tail points towards δ).

129 *Docking.* Binding energy changes in hold, AC_{LA}=AC_{HA} (Fig 1B). To understand the structural
130 underpinnings, we began by removing α-bungarotoxin from the high-resolution (2.69 Å)
131 structure 6UWZ (Rahman et al., 2020) and docking agonists into the empty pocket at the α-δ
132 subunit interface (Fig. 1C). The docking simulations had strong binding scores, ranging from -5.82
133 to -9.18 kcal/mol, suggesting stable interactions. However, unlike the agonist orientation
134 apparent in cryo-EM structures of desensitized AChRs (Gharpure et al., 2019; Noviello et al.,
135 2021; Rahman et al., 2022; Walsh et al., 2018; Zarkadas et al., 2022) (Fig. 1D), the agonist's tail
136 pointed away from (*cis*) rather than towards (t*rans*) the complimentary (non-α) subunit. This was
137 the case for the top 3 docking scores for all 4 ligands (Fig. 2A). Because the *cis* orientation was
138 not observed in any cryo-EM (HA) structure, we examined the top 200 docking scores for CCh. All
139 poses were *cis*, with the tail pointing towards the α subunit. The *cis* orientation was also apparent
140 in docking of agonist into a putatively LA binding site of a homology model (Tripathy et al., 2019).
141 To start, we associated the agonist orientation in the hold end states as *cis* in AC_{LA} versus *trans* in
142 AC_{HA}.
143
144

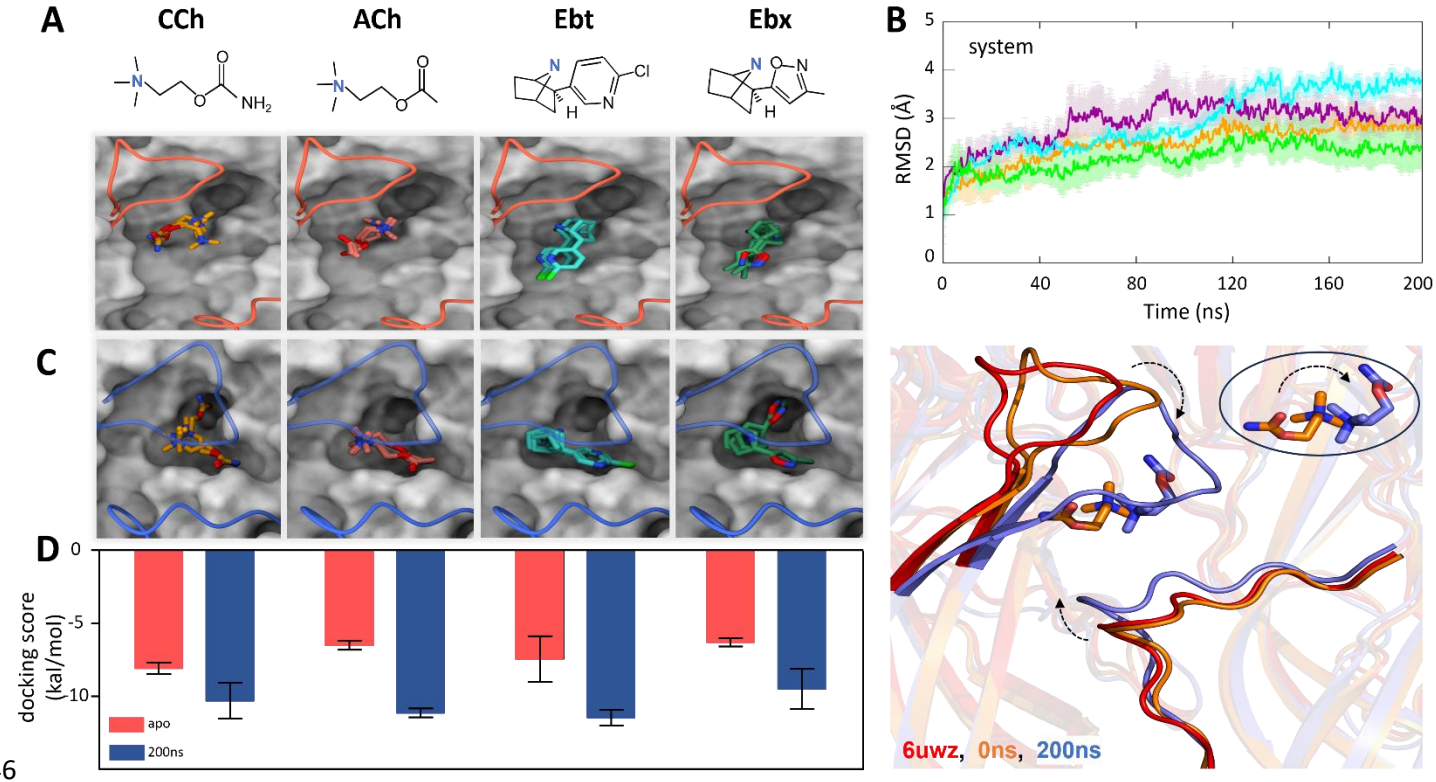

Figure 2. Agonist docking and dynamics. A. *top,* Agonist structures (blue, main N^+): carbamylcholine (CCh), acetylcholine (ACh), epibatidine (Ebt) and epiboxidine (Ebx). B. *top*, root-mean-square-deviation (RMSD) of the system C_α (mean±SD, triplicates) throughout 200 ns MD simulations (ACh, cyan; CCh, green; Ebt, orange; Ebx, purple). *bottom*, close-up view of the pocket showing movements during MD simulations with CCh (red, apo; orange, 0 ns; blue, 200 ns;). Loop C moves down, loop F closes in, the agonist rotates *cis*→*trans.* C. α–δ binding pocket (6UVW.pdb minus toxin) with agonists (top 3 poses). *top*, docked into the 0 ns structure (red). Loop C is up, loop F is out, agonist is *cis*. *bottom*, docked into the 200 ns structure after removing CCh (blue). Loop C is down, loop F is in and the agonist is *trans*. D. Docking score energies (mean±SD), 0 ns (red) and 200 ns (blue) suggest a LA→HA transition during the course of the simulation.

158 *LA→HA transition.* We performed 200 ns MD simulations for each of the docked complexes, in
159 triplicate (with different seed values) (Fig. 2B top). The MD simulations for all three replicates
160 demonstrated similar root-mean-square-deviation (RMSD) patterns, with differences consistently
161 below 1Å (Table S1) suggesting that the trajectories were robust and reproducible. Although there
162 were initial deviations, all systems became stable by ~120 ns. The root-mean-square-fluctuation
163 (RMSF) of the C_α atoms, employed to identify regions of flexibility, showed instability mainly in
164 loops C and F around the pocket (Fig. S2). The fluctuations observed at the base of the ECD were
165 anticipated because the TMD that offers stability here was absent.

166 In addition to the fluctuations in these loops, during the 200 ns simulations the ligand
167 orientation changed dramatically, *cis*-to-*trans*. At the start of the simulations the agonist's tail
168 points towards α, and at the end it points towards δ (Fig. 2B bottom). This rearrangement
169 represents a substantial rotation (a 'flip') about the agonist's main cationic center (N^+) that
170 remains close to αW149 throughout the somersault. The final MD configuration (with CCh) was
171 well-aligned with the CCh-bound cryo-EM desensitized structure (7QL6.PDB) (RMSD < 0.5 Å) (Fig.
172 S3), further demonstrating that the simulation had converged.

173 To test whether rearrangements at the binding pocket in the simulations themselves
174 enforce the *trans* configuration, we removed the bound CCh from the final state MD structure
175 and re-docked all four agonists. The preferred poses for all 4 agonists were all *trans* (Fig. 2C). In
176 addition, binding energies from docking scores were higher for the converged MD structure
177 compared to the initial binding site structure. As a further control we carried out MD simulations
178 of a pentamer docked with ACh and found similar structural changes at the binding pocket
179 compared to the dimer (Fig. S4). These results indicate that a dimer is appropriate to study local
180 rearrangements of an AChR neurotransmitter binding site and suggest that in the MD simulations
181 the binding site restructures from AC_{LA} to AC_{HA} conformation (Fig. 2D).

182

183 *Principal component analysis.* To identify the most prominent conformational states of the
184 receptor during the MD simulations, principal component analysis (PCA) was carried out based
185 on the most significant fluctuations (principal components). Considering the first two principal
186 components (PC-1 and PC-2) that capture the most pronounced C_α displacements, the protein

backbone fluctuations revealed three energy minima (m1, m2, and m3) that mainly reflect the stabilities of loops C and F (Fig. 3). For all four agonists, the trajectories quickly reach m1 ($\leq$20 ns), then transition through m2, and culminate in m3 (180-200 ns). In the simulations progress in time was sequential, m1$\rightarrow$m2$\rightarrow$m3.

Accordingly, we hypothesized that m1 corresponds to AC_{LA} and m3 corresponds to AC_{HA}. For all agonists, the m2 population has greater variance (more instability) compared to m1 and m3. This, along with its position in the sequence, suggests that m2 represents an unstable intermediate configuration within hold, between AC_{LA} and AC_{HA}. For all agonists and trajectories, m3 had the least variance (was most stable), again supporting convergence by 200 ns.

Transitions between the 3 energy minima varied with the agonist. Always, m1 was apparent first (at 5-14 ns for ACh; 15-24 ns for CCh; 21-41 ns for Ebt; 20-56 ns for Ebx), followed by m2 (20-50 ns; 50-60 ns; 60-100 ns; 100-120 ns). All systems converged to m3 (180-200 ns) (Fig. 3). The bottom of the m1, m2 and m3 energy wells represent the most stable configurations of each population and serve as a reference point for the rest of energy well.

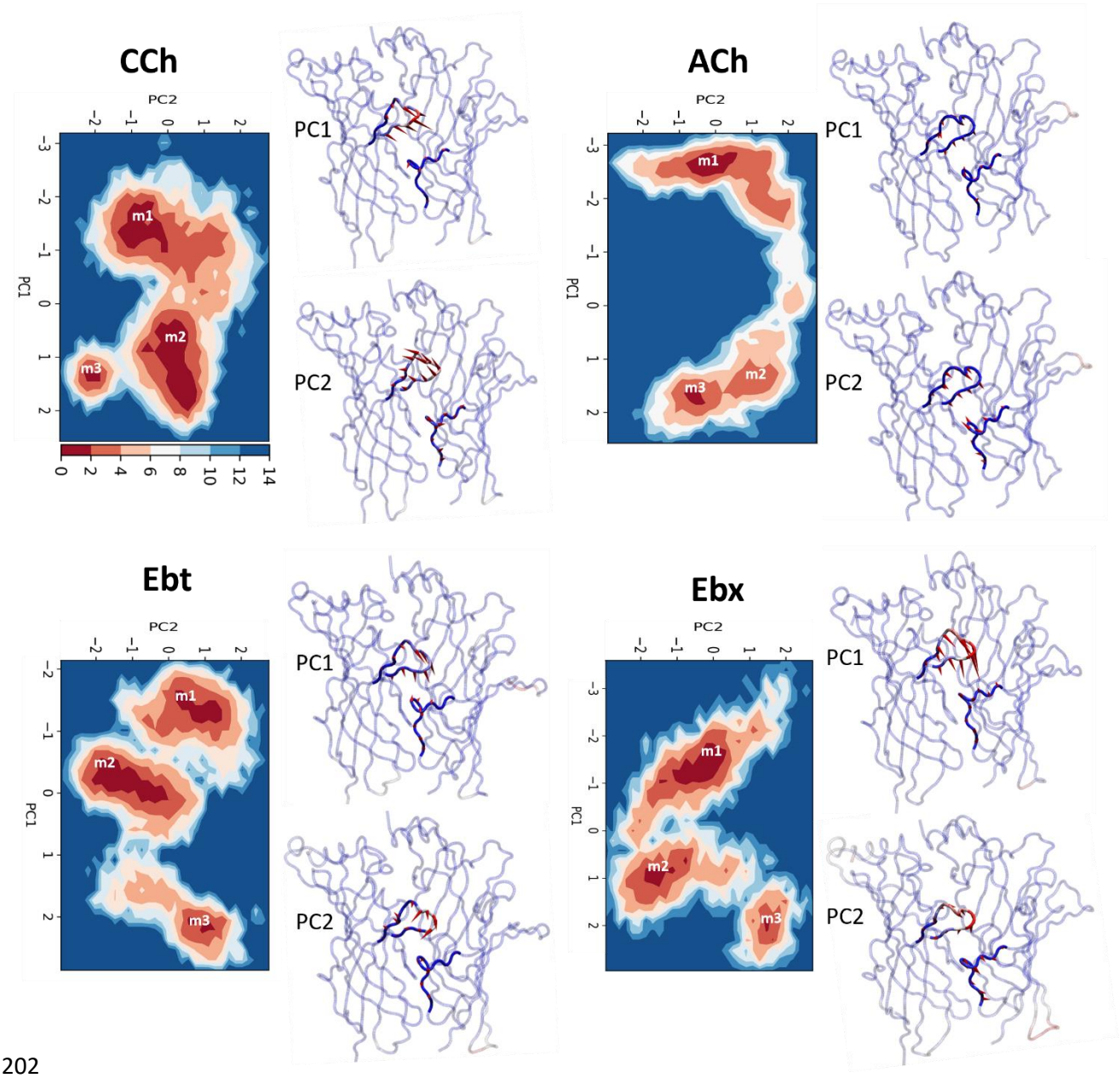

Figure 3. Principal Component Analysis (PCA). For each agonist, the left panel plots PC1 vs PC2, the first two principal components that capture the maximum variance in the trajectory. Colors represent free energy value in kcal/mol (upper left, bottom). For all agonists there are 3 energy minima (red), m1, m2, and m3, that correspond to different conformations of the protein-ligand complex. The right panels are 'porcupine' plots that indicate the direction and magnitude of changes between PC1 and PC2. In order of appearance, m1 ($\leq$20 ns)< m2<m3 ($\geq$180 ns) (see text). m1 represents AC_{LA}, m3 represents AC_{HA}, and m2 is an intermediate configuration (corresponding ΔGs given in Table 1).

209 Although the bottom of the well for 3 energy minima from PCA represent the most stable
210 overall conformation of the protein, they do not convey direct information regarding agonist
211 stability or orientation. To incorporate this information, we performed a cluster analysis of the
212 ligand using frames from the bottom of each PCA well as inputs. The top three clusters, each
213 having RMSD of ≤ 1Å, shared a similar ligand orientation (Fig. S5) and were selected to compute
214 binding free energy using MM-PBSA. The remaining frames were disregarded. The fraction of
215 frames accepted for free energy calculations ranged from a minimum of 20% (ACh, m1) to a
216 maximum of 71% (Ebt, m3). On average, the fraction of frames selected from each energy
217 minimum was ~50%, showing the dynamic nature of the ligand in the pocket (Table 1).
218
219 *Computed vs experimental binding energies.* The above procedure defined populations of
220 structures that we hypothesize represent the end states of hold, AC_{LA} (m1) and AC_{HA} (m3), plus
221 an intermediate (m2). We used MM-PBSA (Molecular Mechanics Poisson-Boltzmann Surface
222 Area) computations of the selected structures to estimate binding energy of each agonist to each
223 population. MM-PBSA is particularly useful to compare binding affinities between different states
224 and among agonists (Kollman et al., 2000; Rastelli et al., 2010; Sun et al., 2014). In our use, MM-
225 PBSA computations included both enthalpic (ΔH) contributions from molecular interactions (van
226 der Waals, electrostatics, solvation) and entropic (TΔS) contributions calculated using normal
227 mode analysis. By capturing the dynamic interplay between the ligand and receptor as well as the
228 influence of the surrounding solvent environment this approach enables computation of a Gibbs
229 free energy (ΔG). However, there are limitations with regard to MM-PBSA accurately predicting
230 absolute binding free energies (Genheden & Ryde, 2015; Hou et al., 2011) that depends on
231 parameterization of the ligand (Oostenbrink et al., 2004).
232 The calculated and experimental ΔG values are shown in Table 1. For ACh and CCh, there
233 is good agreement between ΔG_{m1} and ΔG_{LA} and between ΔG_{m3} and ΔG_{HA}. For these agonists, *in*
234 *silico* values overestimated experimental ones only by ~8% and ~25%. The agreement was not as
235 good for the other 2 agonists, as calculated values overestimated experimental ones by ~45%
236 (Ebt) and ~130% (Ebt). However, the fractional overestimation was approximately the same for
237 ΔG_{LA} and ΔG_{HA}.

Despite these discrepancies in absolute values, the trend of an increase in binding free energy, m1 versus m3, is consistent with the assignment, AC_{LA} versus AC_{HA}. For all agonists, the stability of the ligand-receptor complex increases significantly in the m1→m3 transition (Fig. 4A). Further support for the assignment is from comparing calculated vs experimental efficiencies (η) that depend on $\Delta G_{LA}/\Delta G_{HA}$ (Nayak et al., 2019). Table 2 shows that η values calculated *in silico* agree closely ($\leq$5%) with those measured experimentally, for all agonists. Apparently, MD simulations of a single pdb file successfully model the hold transition. The match between calculated and experimental efficiencies is evidence that that m1 represents low-affinity AC_{LA} and m3 represents high-affinity AC_{HA}.

In the $AC_{LA} \rightarrow AC_{HA}$ conformational change, all agonists show an increase in van der Waals (vdW) interaction energy. The increase was most pronounced with Ebt (-9.77 kcal/mol) and least for Ebx (-3.54 kcal/mol), with CCh (-8.81 kcal/mol) and ACh (-6.71 kcal/mol) falling in between (Fig. 4, Table S2). Also, in $AC_{LA} \rightarrow AC_{HA}$, restructuring of the binding pocket further contribute to generating a smaller, more-tightly packed pocket. This is shown in Fig. 4C as a reduction in binding pocket volume and in Fig. 4D as a decrease in the number of water molecules. The agonist's flip into the pocket results in de-wetting and a more hydrophobic environment.

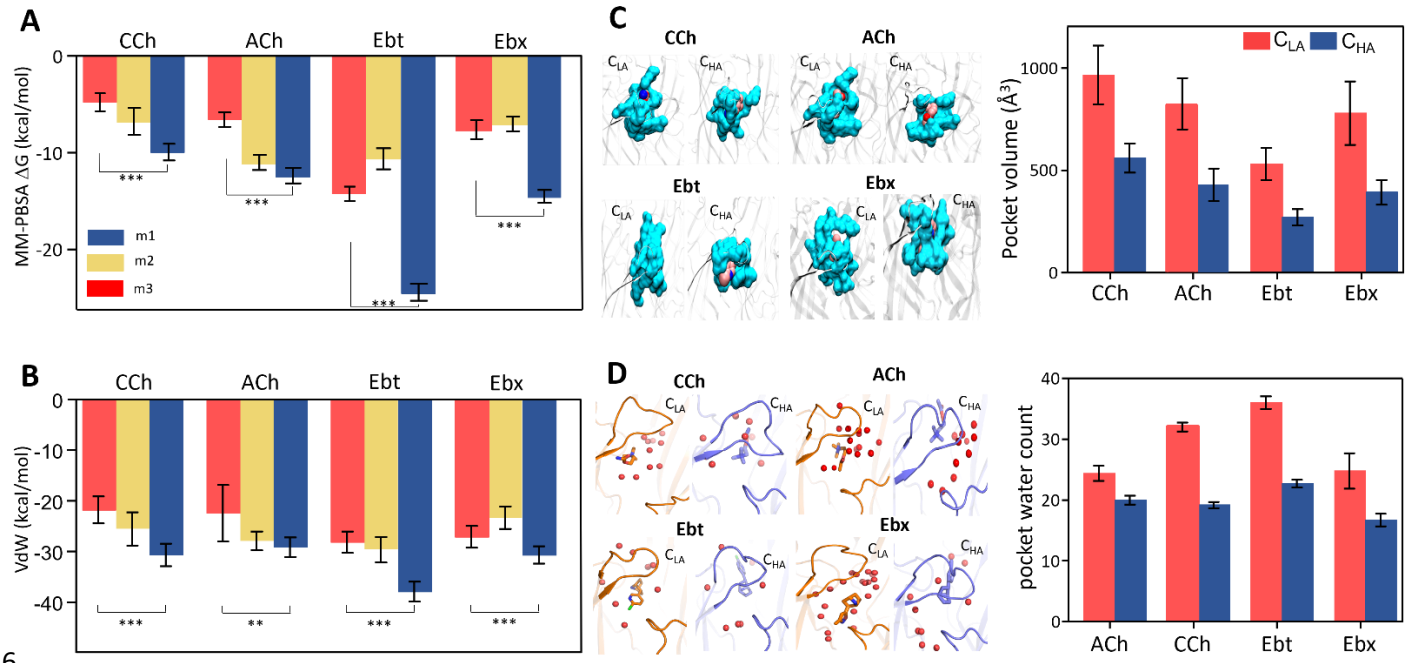

Figure 4. Binding free energies and pocket properties. A. Calculated Gibbs free energy (ΔG) using MM-PBSA for the three distinct energy minima (m1, m2, and m3) showing the progression LA to HA (agonists, Fig. 2A). ΔG_{m2} is intermediate for ACh and CCh but least stable for Ebt and Ebx. B. vdW interactions increase m1 (AC_{LA}) to m3 (AC_{HA}), consistent with increased hydrophobicity. C. Binding pocket volume reduces m1 to m3, reflecting the more tightly packed pocket in AC_{HA}. D. The number of water molecules in the pocket decreases m1→m3, orange, C_{LA}; blue, C_{HA}, reflecting a more hydrophobic environment in AC_{HA}.

Table 1. Calculated and experimental binding energies (kcal/mol).

		window (ns)	n clusters	ΔH (SD, SEM)	TΔS (SD, SEM)	ΔG calculated	ΔG experimental	η calculated	η experimental
	m1	15-24	226	-27.61 (7.66, 0.49)	-22.88 (5.82, 2.37)	-4.73	-4.44		
CCh	**m2**	100-120	273	-24.41 (5.68, 0.79)	-17.54 (3.49, 1.42)	-6.87		0.52	0.52
	m3	186-200	207	-26.18 (5.75, 0.47)	-16.25 (7.76, 2.24)	-9.93	-9.20		
	m1	5-14	100	-20.83 (8.11, 1.13)	-14.27 (6.51, 3.25)	-6.56	-5.11		
ACh	**m2**	20-50	359	-27.92 (3.01, 0.29)	-16.72 (2.53, 1.03)	-11.2		0.47	0.50
	m3	160-200	266	-27.00 (2.88, 0.87)	-14.57 (6.28, 3.63)	-12.43	-10.31		
	m1	21-41	591	-27.64 (3.83, 0.27)	-13.42 (4.70, 1.42)	-14.22	-6.20		
Ebt	**m2**	50-60	325	-24.21 (4.25, 0.42)	-13.50 (6.81, 2.05)	-10.71		0.42	0.42
	m3	175-200	996	-41.77 (3.99, 0.28)	-17.23 (6.86, 2.07)	-24.54	-10.60		
	m1	20-56	1284	-20.51 (2.98, 0.46)	-12.85 (5.49, 1.66)	-7.66	-5.40		
Ebx	**m2**	60-100	504	-21.55 (3.56, 0.28)	-14.39 (10.46, 3.15)	-7.16		0.48	0.46
	m3	174-200	562	-33.95 (2.92, 0.88)	-19.33 (4.39, 1.32)	-14.62	-9.96		

Agonists, see Fig. 2A. For the *values* calculated *in silico*, frames from each PCA population (m1, m2 and m3; Fig. 3) were selected after cluster analysis of ligand orientation. Methods for the experimental energy values are described elsewhere (Indurthi & Auerbach, 2021). window, frame times for each population; ΔH, change in binding enthalpy; ΔS change in binding entropy (T, absolute temperature); ΔH, change in Gibbs free energy (ΔG=ΔH -TΔS); η, efficiency ($1-\Delta G_{LA}/\Delta G_{HA}$). SD, standard deviation; SEM, standard error of mean.

273 *Flip-Flop*. The ligand somersault (flip) was prominent in all simulations of hold. All agonists
274 undergo a large rotation about the N^+-αW149 fulcrum (Fig. 5; Video 1). The extent of rotation
275 was 131° for CCh, 156° for ACh, 148° for Ebt and 176° for Ebx. Another consistent and prominent
276 restructuring event in $AC_{LA} \rightarrow AC_{HA}$ was the downward displacement (flop) of loop C toward the
277 core of the pocket. This movement is conserved in related receptors and thought to play a role in
278 receptor activation by agonists (Basak et al., 2020; Hansen et al., 2005; Hibbs et al., 2009) (see
279 below). In the simulations, we quantified loop C flop by measuring the displacement of its tip (C_α
280 of αC192) relative to its starting position (at 0 ns). The distance traveled at 200 ns varied with the
281 agonist and was 9.2 Å for CCh, 5.5 Å for Ebt, 5.2 Å for ACh and 3.3 Å for Ebx (Fig. 5). We do not
282 discern a pattern with regard to agonist affinity, efficacy or efficiency.

283 In hold, residues that form the pocket cavity move, apparently to accommodate the re-
284 orientation of the ligand. In AC_{LA} αY190, αY93, and δW57 are spaced apart, providing an open
285 slot that accommodates the agonist's tail in the *cis* orientation. However, in AC_{HA} αY190 is
286 positioned closer to αY93, effectively creating a unified surface that disallows the *cis* position of
287 the tail (Fig. S6). However, in the simulations the event sequence is not clear so perhaps flip
288 precedes flop, and agonist re-orientation first creates the space for αY190 to occupy.
289
290

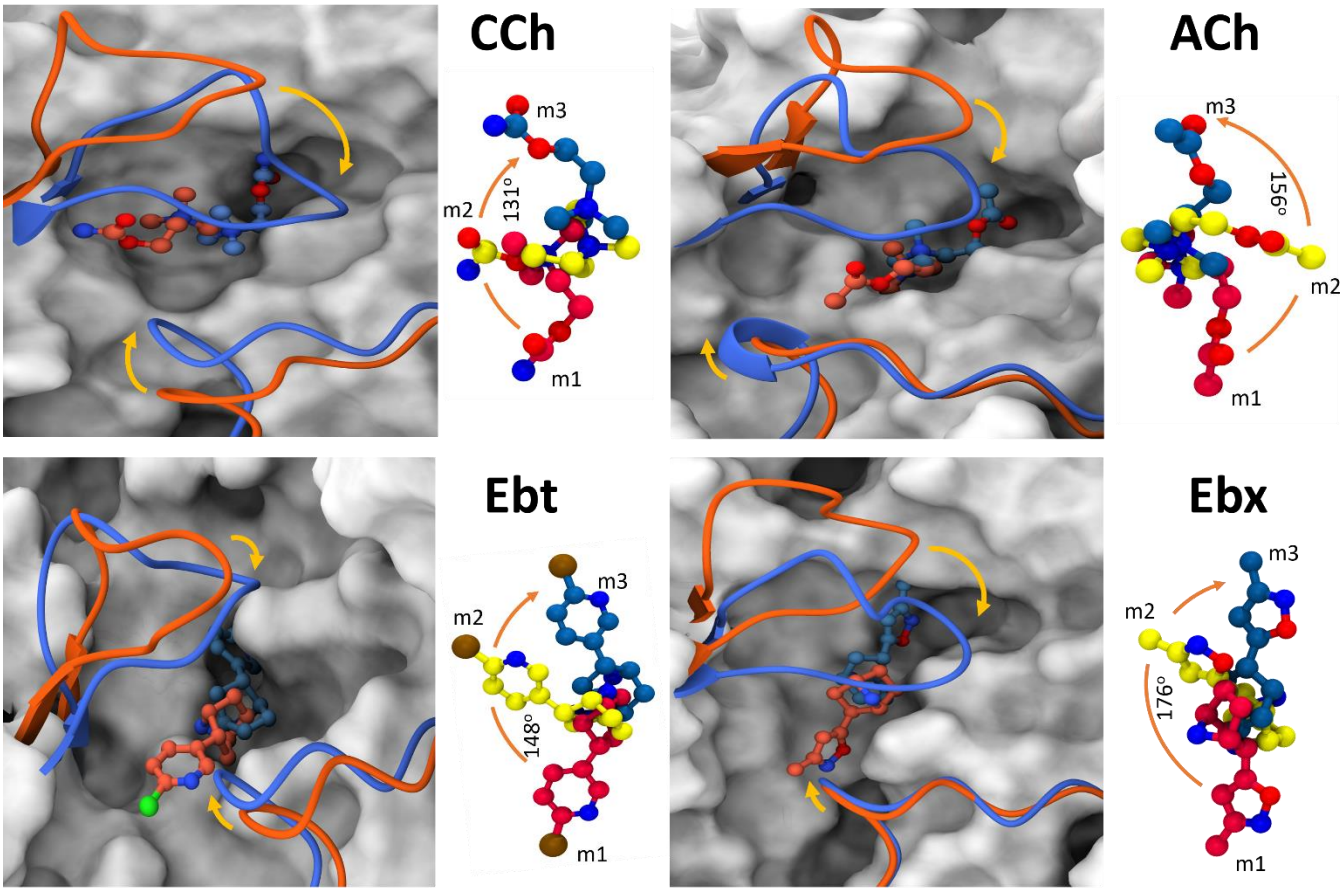

Figure 5. Agonist and loop movements in hold. In each panel, *left***,** superimposed cartoons of AC_{LA} (m1; orange) and AC_{HA} (m3; blue). Loop C is upper left and loop F is lower right. In AC_{LA}→AC_{HA} (orange→blue) there is a *cis*→*trans* reorientation of the agonist (a flip) and a downward movement of loop C (a flop). *right*, the degree of flip from m1 (red) to m2 (yellow) to m3 (blue). The range, m1 (AC_{LA}) →m3 (AC_{HA}), is 131° to 176°.

αW149 (in loop B) makes a cation-π bond with N^+ that is important for ligand stabilization (Xiu et al., 2009; Zhong et al., 1998). In the simulations, the position and orientation of αW149 relative to N^+ remained almost unchanged for all 4 agonists, in both AC_{LA} (*cis*) and AC_{HA} (*trans*) configurations (Fig. 6). Apparently, the cation-π bond acts as a slippery anchor that maintains stability of the N^+ position even as the tail rotates about it.

Loop C flop results in re-positioning of αY190 into the aromatic pocket. αY190 is the main ligand binding energy source, nearly twice as strong as αW149 (Purohit et al., 2014), perhaps because deprotonation of its hydroxyl group generates a cation-anion bond with N^+ (Bruhova & Auerbach, 2017). An interaction between αY190 and the αK145-αD200 salt bridge, suggested to be the trigger for the gating isomerization (Bruhova & Auerbach, 2017; Mukhtasimova et al., 2005). In $AC_{LA}\rightarrow AC_{HA}$, loop C flop restructures the pocket to put N^+ between the αY190 and αW149 rings, and αY190 closer to the salt bridge (Fig. 6).

Other hold rearrangements. In AC_{LA} (m1), the *cis* orientation is stabilized by the hydroxyl of αY93 that is proximal to a functional group on the agonist tail. Also, the tail nitrogen in CCh, Ebt, and Ebx (amide or amine) forms a hydrogen bond with the hydroxyl group of αY198, but only in the intermediate m2 state. This interaction appears to guide the flip and provide transient stability to the intermediate state. The absence of a secondary nitrogen in ACh possibly explains its alternate re-orientation route, as only this ligand was observed to flip counterclockwise (Fig. 5). It may also explain why the m2 basin in the PCA plots for ACh is especially broad and shallow (Fig. 3).

In AC_{HA} (m3), the αY190/αY198/δW57 rings and the αW149 indole interact with N^+, and the hydroxyl group of αY93 forms a hydrogen bond with the ligand head group (Celie et al., 2004; Hansen et al., 2005). However, Ala substitutions of these 5 aromatic residues have quite different consequences and result ACh binding free energy losses of +4.4, +1.9, +0.1, +2.3 and +0.9 kcal/mol, respectively (Purohit et al., 2014). In AC_{HA}, the tail functional moiety (carbonyl or secondary ring amine) in the *trans* orientation is sandwiched between αC192, αC193 and αY198 (loop C), αT150 (loop B) and δC108, δN109, δL111, and δL121 (loop E) (Fig. S7).

αK145 is complex and undergoes agonist-dependent hold rearrangements. In AC_{HA} this residue i) makes a salt bridge with αD200, ii) has a cation-π interaction with αY93, iii) contacts

αY190 (possibly through the hydroxyl group) and iv) approaches loop F of the complementary subunit (Zarkadas et al., 2022). Further, the mutation αK145A lowers the efficiencies of ACh and CCh (from 0.51 to 0.41) but has no effect on those of Ebt and Ebx (0.41) (Indurthi & Auerbach, 2023).

This agonist dependence with regard to function has a parallel in structure. In the hold simulations, the αK145-αD200 distance (Å) increases from 4.4 in apo to 6.1 or 5.1 in AC_{LA} (CCh or ACh). The spread may relate to the agonist tail being inserted into the αY93 slot in the *cis* orientation. In $AC_{LA} \rightarrow AC_{HA}$, for some agonist the αK145-αD200 distance (Å) shortens substantially to 2.6 or 2.8, making the bridge more rigid (ACh or CCh). However, with Ebt and Ebx the αK145-αD200 distance remains unstable, fluctuating between 3-6 Å throughout the course of the simulation. Likewise, αK145-αY190 distance stabilizes at 5.3 Å or 6.1 Å in AC_{HA} with ACh and CCh but continues to fluctuate with Ebt and Ebx. In contrast, the αY190-αD200 distance remains stable in AC_{HA} for all ligands. This suggests that the instability in the salt αK145-αD200 and αK145-αY190 distances can primarily be attributed to αK145 (Fig. S8).

In AC_{HA}, the functional group found in the tail of each agonist -- the carbonyl group in CCh and ACh and the secondary ring amine in Ebt and Ebx - forms a hydrogen bond with the carbonyl of δN109 and the amine of δL121 in the complementary δ subunit *via* a structural water (Fig. 6), as reported elsewhere (Blum et al., 2010; Gharpure et al., 2019; Zarkadas et al., 2022). This water-mediated bonding appears to be crucial for stabilizing the agonist in the *trans* orientation. The start of the agonist's flip, m1→m2, begins the establishment of this water-mediated bond that is completed in m2→m3, with all 4 agonists (Fig. 6).

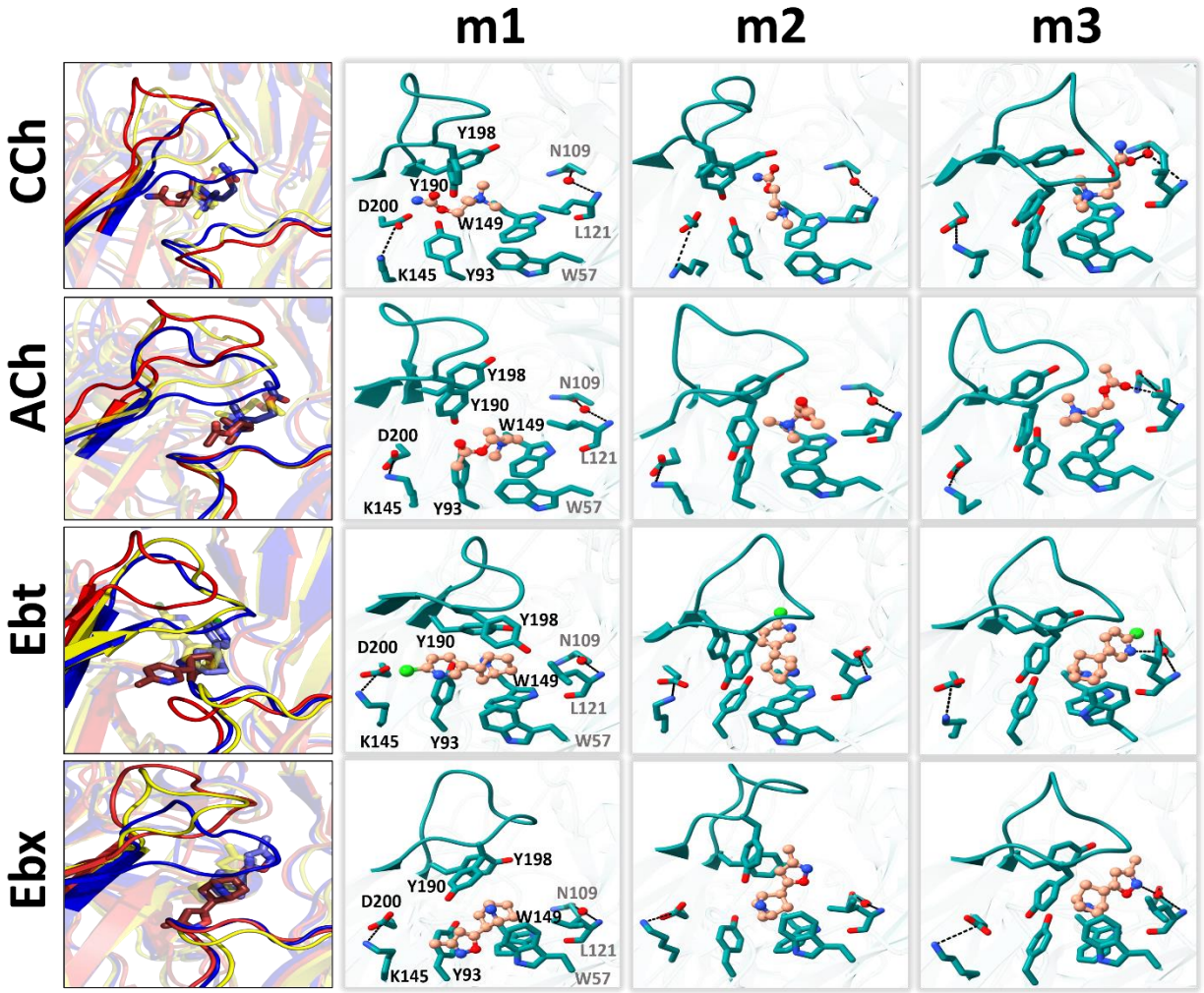

Fig. 6: Representative snapshots in hold. *left*, rearrangements of loop C, loop F and the ligand (m1, red; m2, yellow; m3, blue). Right, conserved residues and ligand orientation. m1 is AC_{LA} and m3 is AC_{HA}. In m1, a functional group at the agonist tail interact with αY93 (all agonists) and αD200 (CCh and Ebt). The position and orientation of αW149 relative to N^+ of the agonist remains unchanged m1→m3 and serves as a fulcrum for the *cis*→*trans* flip (see Fig. 5). In m2, the functional nitrogen at the agonist tail (CCh, Ebt and Ebx) interacts with the hydroxyl group of αY198. For all ligands, loop C flop (m1→m3) repositions αY190 in pocket. In m3, the agonist fully flips to *trans*, facilitating the interaction of N^+ with αY190 and the formation of water-mediated hydrogen bond with the reactive group at the tail with δN109/δL121 (loop E).

Discussion

In diffusion-catch-hold activation of AChRs ($A+C \rightleftarrows {}^{A}C \rightleftarrows AC_{LA} \rightleftarrows AC_{HA}$; Fig. 1B), the binding free energy increase in the last step generates the force that initiates the receptor isomerization. We identified in MD simulations (Fig. 3) the hold end states, AC_{LA} (m1) and AC_{HA}, (m3), as well as an intermediate configuration (m2). Our approach to understanding the conformational dynamics of hold is to compare calculated with experimental binding free energies, ΔG_{LA} and ΔG_{HA}. There are many experimental measurements for many different AChR agonists and several binding sites (Indurthi & Auerbach, 2023; Jadey & Auerbach, 2012; Purohit et al., 2014), but here we describe the comparison for only 4 agonists and only the wt $\alpha-\delta$ site.

The alignment between experimental and calculated free energies was closer for ACh and CCh than for Ebt and Ebx (Table 1). The match improved when free energy ratios rather than absolute values were compared. Individual *in silico* values overestimated experimental ones by approximately the same factor (different for each ligand) that, however, cancelled in the ratio. We do not know the origin of this factor but speculate that it could be caused by errors in ligand parameterization. Regardless, the results show that agonist efficiency (η) can be estimated from only agonist and receptor structure (one PDB file), and that η is a useful metric for associating structure with function.

In the $AC_{LA} \rightarrow AC_{HA}$ simulations, two conspicuous binding site rearrangements were a *cis*$\rightarrow$*trans* somersault of the agonist (a flip) and an up$\rightarrow$down droop of loop C (a flop). The loop C movement is well known, but its functional role has been puzzling. The extent of the flop is correlated with agonist potency in ACh binding proteins (Basak et al., 2020; Du et al., 2015; Polovinkin et al., 2018), but voltage-clamp fluorometry of other receptors shows it to be similar with agonists and antagonists (Chang & Weiss, 2002; Munro et al., 2019; Pless & Lynch, 2009). In AChRs, truncation of loop C prevents activation by agonists but has no effect on unliganded activation, but agonist sensitivity is maintained if αY190 and αY198 are intact (Purohit & Auerbach, 2013). These results suggest that the downward displacement of loop C in AChRs is mainly associated with the generation of strong binding energy.

Perhaps the most puzzling result regarding loop C is that the agonist association rate constant k_{on} is slower to AC_{LA} (up position) than to AC_{HA} (down position) (Grosman & Auerbach,

391 2001; Nayak & Auerbach, 2017). Moreover, whereas k_{on} to AC_{LA} is correlated with agonist potency
392 (the dissociation rate constant k_{off} is approximately the same for all agonists), k_{on} and k_{off} to AC_{HA}
393 both are agonist dependent. The flop of loop C in hold removes a barrier to make k_{on}
394 approximately diffusion-limited, and also reduces discrimination between ligands (molecular
395 recognition.

396 Loop C droop resembles the 'clamshell closure' apparent at other receptors binding site
397 (Chen et al., 2017; Hansen et al., 2005; Hibbs & Gouaux, 2011). However, in the light of the above
398 experimental results, this label is misleading because 'closing' (or 'capping') a binding pocket is
399 expected to slow rather than speed k_{on}. For this reason, we use less functionally loaded words to
400 describe the downward displacement of loop C, namely a 'flop' or 'droop'. In $AC_{LA}\rightarrow AC_{HA}$ loop C
401 indeed moves closer to αC of αW149, to cover the pocket and create higher affinity. However, it
402 does not do so by imposing a steric barrier. We did not study the catch rearrangement and do not
403 speculate about the nature of the barrier that limits the agonist association rate constant to C_{LA}
404 that has loop C in an up position.

405 Importantly, loop C flop repositions αY190, the main determinant of both LA and HA
406 binding energies (Bruhova & Auerbach, 2017; Purohit et al., 2014). In $AC_{LA}\rightarrow AC_{HA}$, this side chain
407 fills the slot adjacent to αY93 that otherwise allows the *cis* orientation in AC_{LA} (Fig. S5). Further,
408 flop moves αY190 closer to a salt bridge between αK145-αD200, and compacts the space
409 between αW149 and N^+ (Fig. 6). Overall, the simulated structures suggest that loop C flop
410 increases binding energy both by repositioning αY190 near N^+ and by allowing the *cis-trans* flip
411 of the ligand. Rather than closing a door, the downward movement of loop C rearranges the
412 furniture.

413 We interpret *cis-trans* rotation of the agonist about the N^+-αW149 fulcrum (Fig. 5) with
414 caution. Although the *trans* orientation is apparent in desensitized AChR cryo-EM structures, the
415 *cis* orientation exists only *in silico*. Notwithstanding this limitation, in $AC_{LA}\rightarrow AC_{HA}$ the agonist's flip
416 into the binding pocket and the repositioning αY190 by loop C flop were observed consistently in
417 all simulations with all agonists, and rationalize the increase binding energy in the hold transition.
418 We speculate that the agonist flip triggers the rest of the hold restructuring but cannot rule out

flop promoting flip or synchronous rearrangements. We have been unable to establish clearly the flip-flop temporal sequence.

For the agonists we examined, the somersault positions the tail deep into the binding cavity where it interacts *via* a structural water with the complementary subunit. It appears that agonists rotation increases binding free energy by displacing water and increasing vdW interactions and protein stability. A hydrophobic binding pocket is associated with functional activation in other ion channels (Furukawa et al., 2005; Sigel & Steinmann, 2012) and is observed in many proteins including β2-adrenergic receptor, opioid receptors, and HIV-1 protease (Huang et al., 2015; Rasmussen et al., 2011; Wlodawer & Erickson, 1993). However, these effects on the AChR pocket cannot be the only basis for the higher affinity AC_{HA} because several potent agonists lack a tail, for example tetramethylammonium. We hypothesize that both the reorganization of the aromatic groups in the pocket around N^+ and binding site compaction/de-wetting contribute to stronger binding, in proportions that remain to be determined. Regardless, the agonist's somersault shows that mobility is one feature that distinguishes a ligand from a covalently linked side chain (Indurthi & Auerbach, 2023). Not only can an unconnected agonist come and go, it can also reposition itself dramatically to induce a conformational change of binding pocket to affect a change in binding energy.

Movements analogous to flip and flop have been identified in other proteins. Multiple ligand positions in a binding pocket have been documented in 5-HT3 receptors (Basak et al., 2020), δ-opioid receptors (Shang et al., 2016), HIV-1 protease (Klei et al., 2007) and transthyretin (Klabunde et al., 2000). In enzymes, substrate motion has been observed in hexokinase (Bennett & Steitz, 1978) and alcohol dehydrogenase (Plapp, 2010). Regarding flop, substrate-induced loop displacements are known to reposition residues to enhance catalysis, for example in chymotrypsin (Ma et al., 2005) and triosephosphate isomerase (Brown & Kollman, 1987; Nickbarg et al., 1988). The agonist flip and loop C flop in AChRs are additional examples of ligand mobility and loop motions undergirding function.

The PCA plots (Fig. 3) show 3 structural populations, one of which (m2) occurs in time between m1 (AC_{LA}) and m3 (AC_{HA}). In m2, the agonist tail interacts with αY198, possibly to guide the clockwise rotation of the ligand and reduce the probability of a return to the *cis* orientation.

448 ACh was the only agonist to rotate counterclockwise, perhaps because it lacks the appropriate
449 functional group in its tail. The MM-PBSA calculations indicate that ΔG_{m2} (that does not have an
450 experimental correlate) is intermediate between ΔG_{LA} and ΔG_{HA} for ACh and CCh, but least stable
451 for Ebt and Ebx (Table 1). We do not have an explanation for this difference. However, we observe
452 m1→m2, m2→m1, m2→m3 and m3→m1 transitions in the trajectories (Video 1), so the depth
453 of the m2 energy well (relative to the barriers that separate it from m1 and m2) contributes to
454 agonist efficacy and efficiency.

455 MD simulations did not reveal an interaction between the αK145-αD200 salt bridge
456 distance and the degree of loop C displacement (Cheng et al., 2006). However, this distance
457 discriminate between η classes by decreasing AC_{LA}→AC_{HA} in high (ACh and CCh) but not in low
458 (Ebt and Ebx) η classes, consistent with experimental results (Indurthi & Auerbach, 2023). All 4
459 agonists are high efficacy, so this result suggests that perturbation of this salt bridge is not a
460 necessary requirement for the change from LA to HA. After loop C flop, the repositioned αY190
461 connects N^+ to the salt bridge, suggesting that this interaction (rather than bridge tightening)
462 could help trigger the gating transition (Beene et al., 2002; Gay & Yakel, 2007; Mukhtasimova et
463 al., 2005; Padgett et al., 2007; Pless et al., 2011). The simulation did not reveal the
464 conformational changes (forces) that drive the next step of the isomerization (ECD
465 restructuring). However, the observation that for all agonists, interactions with the
466 complementary subunit and pocket dehydration terminated (at 200 ns) the hold rearrangement
467 lead us to speculate these may contribute.

468 Loop E (connecting β5 and β6 strands) has been implicated in ligand discrimination (Basak
469 et al., 2020; Muroi et al., 2009; Pless & Lynch, 2009). The double mutation F106L+S108C in the
470 β2 subunit of the α4β2 nicotinic AChR subtype significantly decreases the action of Ebt without
471 altering that of ACh (Tarvin et al., 2017). Loop E residues are responsible for the binding energy
472 difference of α–γ versus α–δ interfaces because hydrogen bonds influence the position and
473 participation of γW55 (Nayak et al., 2016), and for reducing instability of the α–δ site consequent
474 to loop C mutations (Purohit & Auerbach, 2013). MD simulations with more agonists and more
475 binding sites are needed to elucidate the role of loop E in the AC_{LA}→AC_{HA} transition.

Agonists belong to efficiency (η) classes in which $\Delta G_{LA}/\Delta G_{HA}$ is the same for all members. So far 5 η-classes have been identified experimentally in adult-type AChRs, indicating that are 5 pairs of AC_{LA}/AC_{HA} structures (Indurthi & Auerbach, 2023). Although in the simulations loop F movements and salt bridge distances were agonist dependent, with only 4 ligands we cannot associate these rearrangements with η classes.

The key requirement for allostery is that ligand binding energy be weaker to the resting versus active conformation of the target. Natural selection must generate both low and high affinity binding sites, so our attention must be on restructuring in both $^{A}C=AC_{LA}$ (catch) and $AC_{LA}=AC_{HA}$ (hold). What prevents loop C flop in apo? What barrier(s) slows k_{on} to apo? Where is the agonist in the encounter complex? What forces promote the *cis* orientation? What is the role of water in agonist orientation, both *cis* and *trans*? What are the mechanisms and consequences of a wider salt bridge, apo versus AC_{LA}? What structural classes are associated with efficiency classes? The correlation in the free energy changes in catch and hold that entangles binding with gating implies a corresponding correlation in structural change. We anticipate that additional MD simulations of catch, hold, and post-hold domain rearrangements, for more agonists and with binding site mutations, will lead to a more complete understanding of how agonists turn on the AChR.

Materials and Methods

Hardware and Software. All computational studies were carried out on a Linux Ubuntu 20.04 based workstation with 126 GB RAM, 64 CPU cores, and two RTX A5000 24 GB GPU cards, as well as an Ubuntu 20.04 based server equipped with 132 GB RAM, 96 CPU cores, and two RTX A5000 24 GB GPU cards. The software utilized includes the Maestro release 2022-2 graphical user interface (GUI) of the Schrödinger software suite (BioLuminate, Schrödinger, LLC, NY, USA), Amber22 (Case et al., 2005), VMD 1.9.3 (Humphrey et al., 1996), ChemDraw Professional 15.1 (Purushotham et al., 2022), ChimeraX (Pettersen et al., 2021), and PyMOL (PyMOL Molecular Graphics System, Version 2.0, Schrödinger, LLC).

Protein preparation. Protein preparation was conducted using the Protein Preparation Wizard (PPW) (Purushotham et al., 2022) and OPLS4 force field. Bond orders were assigned to atoms based on the CCD database, with zero bond orders given to bonded metals. Missing hydrogen atoms were inserted, and disulfide bonds were placed appropriately. During preprocessing, structural refinement was performed with Maestro's Prime utility, optimizing and adding any missing side chains and residues. Missing residues were formulated by combining SEQRS information from the PDB files and optimized using Prime's ePLOP module. The ionization state of all heterogeneous groups, including ligands, bound metals, and charged amino acids, were determined using the EpiK tool at a pH range of 7.0 ± 2.0. Subsequent force field minimization allowed for water sampling and basic restraint minimization, during which only hydrogen atoms could be freely reduced.

The hydrogen bonding (H-bond) network underwent significant modification. The terminal chi angle for Asn, Gln, and His was sampled through 180-degree flips, altering their spatial H-bonding capabilities without affecting the fit to electron density. The neutral and protonated states of His, Asp, and Glu, as well as two His tautomers, were sampled. Hydrogens on hydroxyls and thiols were also analyzed to enhance the H-bond network. Finally, the ProtAssign method was employed in two modes: a "regular" mode, which completed in seconds, and an "exhaustive" mode that considered many more states and could take minutes or hours, depending on the H-bond network complexity.

Ligand Preparation. The two-dimensional SDF structures of carbamylcholine (CCh), acetylcholine (ACh), epibatidine (Ebt) and epiboxidine (Ebx) were retrieved from the PUBCHEM database. LigPrep (LigPrep, Maestro 11.2.014, Schrödinger LLC) was utilized to construct ligands, produce stereoisomers, and generate tautomers using the OPLS46 force field. Additionally, the Epik module was employed to desalt and protonate the ligands at pH 7.0. Default values were applied to the remaining parameters, and LigPrep was also used to prepare the ligands ACh, CCh, Ebt, and Ebx, with the option "retain specified chiralities" engaged.

In terms of ligand state assessment, Epik can calculate a penalty to quantify the energy cost of forming each state in solution based on the Hammett and Taft methods. This EpiK state penalty is entirely compatible with the GlideScore used for docking, as it is computed in kcal/mol units. This compatibility facilitates the examination of how the EpiK state penalty affects the GlideScore. The DockingScore in Glide represents the total of the GlideScore and the Epik state penalty and served as the basis for final ranking and enrichment evaluation. Furthermore, Epik offers a technique for handling metal binding states, involving a change in the pH range within which the state is generated. This approach underscores the comprehensive considerations made in preparing the ligands for docking and subsequent analyses.

Grid Generation and Molecular Docking. The receptor grid complex of 6UWZ.pdb was generated after removing alpha-bungarotoxin from the binding pocket using Glide (Glide, Maestro 11.2.014, Schrödinger LLC). A virtual grid box with dimensions 20Å × 20Å × 20 Å was formed, centered within the C and F loops in the α–δ binding site of the energy-minimized resting state. This grid box was used to generate a receptor grid, and the default values were assigned for other parameters. Docking was performed using the ligand docking wizard built into the Glide module of Schrödinger, with the default scaling factor and partial charge cutoff set to 0.80 and 0.15, respectively. The docking procedure consisted of two stages, extra precision (XP) followed by post-processing with prime MM-GBSA. The best dock poses were selected based on dock score and MM-GBSA energy for further investigation.

Molecular Dynamics Simulations. MD simulations were conducted using the Amber22 software suite within the Amber module as detailed elsewhere (Singh et al., 2021; Srivastava et al., 2022).

Ligand topology was prepared via the Leap module in AmberTools22, employing force field ff19SB (Tian et al., 2020) and the Generalized Amber Force Field (GAFF) (Vassetti et al., 2019). The AM1-BCC strategy and GAFF2 were used to assign atomic charges and additional parameters. Before simulation, the systems were minimized and equilibrated following a five-step minimization process, with each step involving 10,000 energy minimization steps. Systems were heated under NVT ensembles in two consecutive runs from 0–300 K for 1 ns each, followed by a 1 ns simulation at 300 K and 1 bar pressure under the NPT ensemble for equilibration. An additional 5 ns equilibration was performed before the 200 ns production MD for each system, conducted under periodic boundary conditions (PBCs) and utilizing an NPT ensemble with 300 K and 1 bar pressure. Long-range electrostatic interactions were treated using the particle mesh Ewald method (PME), including a direct space cutoff of 12.0 Å and van der Waals interactions. In production MD, a time step of 2.0 fs was employed, and the SHAKE algorithm was used to keep bond lengths at equilibrium. Isobaric (NPT) conditions were maintained using the Berendsen barostat, with temperature monitored by a Langevin thermostat. Coordinates from the production MD were recorded in the trajectory file every 20 ps, resulting in a minimum of 10,000 frames. Trajectories were analyzed using amber-tools CPPTRAJ (Roe & Cheatham, 2013), and further analysis and figure generation were completed with VMD, Pymol, Xmgrace and ChimeraX. To ensure reproducibility, MD trajectories were generated in triplicate.

Cluster Analysis. Cluster analysis of the ligand was performed using TCL scripts within the Visual Molecular Dynamics (VMD) software, as described elsewhere (Mittal, Tonk, et al., 2021). In brief, this script automates the identification of frames from the most stable conformations based on PCA minima. Using these frames as input, the algorithm employed RMSD values of ligand positions to cluster similar orientations. Specifically, clusters with an RMSD of ≤ 1Å were considered to share a similar ligand orientation. Frames that did not fit into these top clusters were automatically excluded by the script.

578 **Principal Component Analysis (PCA) and Free Energy Landscape (FEL).** PCA identifies collective
579 motions in atomic-level simulations of macromolecules (Mittal, Srivastava, et al., 2021; Srivastava
580 et al., 2022). It emphasizes significant patterns by reducing noise in MD simulations, revealing
581 essential dynamics underlying conformational changes. All equilibrated MD simulation
582 trajectories were analyzed by PCA computations using the CPPTRAJ algorithm in Amber tools.

583 Prior to PCA, least-square fitting of the protein's Cα atoms was carried out with respect to
584 a reference structure (average protein coordinates) to eliminate rotational and translational
585 degrees of freedom in the simulation box. A positional covariance matrix C (of dimensions $3N \times$
586 $3N$) was constructed using the Cα atom coordinates, and this matrix was diagonalized to produce
587 eigenvectors (directions of motion) and eigenvalues (magnitudes). The elements of the
588 covariance matrix C were obtained using:

589 $C_i = \langle (X_i - \langle X_i \rangle)(X_j - \langle X_j \rangle) \rangle$ (i, j=1,2,3…….,3N), (Eq. 1)

590 where X_i and X_j are the Cartesian coordinates of the Cα atoms, and N is the number of Cα atoms.
591 The ⟨⟩ notation represents the ensemble average of atomic positions in Cartesian space. The
592 resulting principal components (eigenvectors) were sorted by the total motion they captured,
593 generating 3N eigenvectors. The free energy landscapes (FELs; FIg.3) were created using the
594 "g_sham" module in GROMACS, based on the probability distribution of the top two principal
595 components (PCs). The FEL plot aids in visualizing possible conformations and corresponding
596 energy levels. The free energy values (G) were calculated as

597 $G_i = -kT \ln(N_i/N_{max})$ (Eq. 2)

598 where k is the Boltzmann constant, T is the absolute temperature of the simulated system (300
599 K), N_i is the population of bin i, and N_{max} is the population of the most-populated bin.
600

601 **Binding Free Energy Calculation.** The binding free energy of the protein-ligand docked complex
602 (ΔG_{bind}) was calculated in two stages, after docking (using MM-GBSA in the Prime module of
603 Schrödinger) (Mittal, Tonk, et al., 2021; Purushotham et al., 2022) and after MD simulation on
604 equilibrated MD trajectories (using MM-PBSA/-GBSA in AMBER22) .

After docking, for the static docked pose of the protein-ligand complex the MM-GBSA binding energy calculation was performed using the OPLS4 force field and the variable-dielectric generalized Born (VSGB) model in the Prime MM-GBSA module in Schrödinger 2022. We used ΔG_{bind_dock} to rank protein-ligand docked complexes, selecting those with the highest negative values and dock scores as the best ligands for further studies. After MD Simulation, in the MD-equilibrated system binding energies were calculated through the MM-PBSA/-GBSA protocol, implemented in AMBER22. This was performed over the most stable clustered poses extracted from the equilibrated trajectory at minima m1, m2, and m3 on the free energy landscape (FEL) over a 200 ns time frame. AMBER utilizes the conventional g_mmpbsa module for MM-PBSA calculations using MM-PBSA.py script. These methods calculate the energies of electrostatic interactions, van der Waals interactions, polar solvation, and non-polar solvation in the equilibrated trajectory using a single trajectory protocol (STP). The binding energy of each protein-ligand complex (ΔG_{bind}) was calculated as

$$G_{bind} = \Delta G_{complex} - \Delta G_{protein} - \Delta G_{ligand}$$

where $\Delta G_{complex}$, $\Delta G_{protein}$, and ΔG_{ligand} represent the absolute free energies of the complex, protein, and ligand systems, respectively. Additional terms, such as ΔH (enthalpy), T and ΔS (temperature and total solute entropy), ΔG_{gas} (total gas phase energy), and ΔG_{solv} (solvation energy), contribute to the calculation.

The Poisson-Boltzmann calculations were performed using an internal PBSA solver in Sander, while Generalized Born ESURF was calculated using 'LCPO' surface areas. The vibrational mode entropy contributions ($T\Delta S$) for protein-ligand interactions were calculated and averaged using normal-mode analysis in Amber. The entropy term provides insights into the disorder within the system, as well as how this disorder changes during the binding process. This value was added to the enthalpy term computed by the MM-PBSA method to determine the absolute binding free energy (ΔG_{bind}). These comprehensive calculations allowed for a precise evaluation of the interactions between the protein and ligand, providing valuable insights into the binding process and its energetic characteristics.

633 **Pocket Volume Calculation.** To investigate the variations in binding site volume across all four
634 agonist-bound cases, pocket volume analysis was carried out using POVME3.0 (Wagner et al.,
635 2017). From each of the four systems, frames were extracted at consistent intervals with a stride
636 of 2.0, culminating in representative sets of 5000 protein structures for every system. Before
637 commencing the volume calculation, the trajectory was aligned, and frames were selected from
638 VMD, serving as the initial input for this method. Subsequently, an inclusion region was defined,
639 encapsulating all binding pocket conformations within the trajectory. This region's definition
640 involved building a sphere upon which the inclusion grid-points were computed, using different
641 atoms of the ligand for this calculation.

642 **References:**

643

644 Auerbach, A. (2020). Pathways for nicotinic receptor desensitization. *J Gen Physiol*, *152*(10).
645 https://doi.org/10.1085/jgp.202012639
646 Basak, S., Kumar, A., Ramsey, S., Gibbs, E., Kapoor, A., Filizola, M., & Chakrapani, S. (2020). High-
647 resolution structures of multiple 5-HT(3A)R-setron complexes reveal a novel mechanism of
648 competitive inhibition. *Elife*, *9*. https://doi.org/10.7554/eLife.57870
649 Beene, D. L., Brandt, G. S., Zhong, W., Zacharias, N. M., Lester, H. A., & Dougherty, D. A. (2002). Cation-pi
650 interactions in ligand recognition by serotonergic (5-HT3A) and nicotinic acetylcholine receptors:
651 the anomalous binding properties of nicotine. *Biochemistry*, *41*(32), 10262-10269.
652 https://doi.org/10.1021/bi020266d
653 Bennett, W. S., Jr., & Steitz, T. A. (1978). Glucose-induced conformational change in yeast hexokinase.
654 *Proc Natl Acad Sci U S A*, *75*(10), 4848-4852. https://doi.org/10.1073/pnas.75.10.4848
655 Blum, A. P., Lester, H. A., & Dougherty, D. A. (2010). Nicotinic pharmacophore: the pyridine N of nicotine
656 and carbonyl of acetylcholine hydrogen bond across a subunit interface to a backbone NH. *Proc*
657 *Natl Acad Sci U S A*, *107*(30), 13206-13211. https://doi.org/10.1073/pnas.1007140107
658 Brown, F. K., & Kollman, P. A. (1987). Molecular dynamics simulations of "loop closing" in the enzyme
659 triose phosphate isomerase. *J Mol Biol*, *198*(3), 533-546. https://doi.org/10.1016/0022-
660 2836(87)90298-1
661 Bruhova, I., & Auerbach, A. (2017). Molecular recognition at cholinergic synapses: acetylcholine versus
662 choline. *J Physiol*, *595*(4), 1253-1261. https://doi.org/10.1113/JP273291
663 Case, D. A., Cheatham, T. E., 3rd, Darden, T., Gohlke, H., Luo, R., Merz, K. M., Jr., Onufriev, A., Simmerling,
664 C., Wang, B., & Woods, R. J. (2005). The Amber biomolecular simulation programs. *J Comput*
665 *Chem*, *26*(16), 1668-1688. https://doi.org/10.1002/jcc.20290
666 Celie, P. H., van Rossum-Fikkert, S. E., van Dijk, W. J., Brejc, K., Smit, A. B., & Sixma, T. K. (2004). Nicotine
667 and carbamylcholine binding to nicotinic acetylcholine receptors as studied in AChBP crystal
668 structures. *Neuron*, *41*(6), 907-914. https://doi.org/10.1016/s0896-6273(04)00115-1
669 Chang, Y., & Weiss, D. S. (2002). Site-specific fluorescence reveals distinct structural changes with GABA
670 receptor activation and antagonism. *Nat Neurosci*, *5*(11), 1163-1168.
671 https://doi.org/10.1038/nn926
672 Chen, S., Zhao, Y., Wang, Y., Shekhar, M., Tajkhorshid, E., & Gouaux, E. (2017). Activation and
673 Desensitization Mechanism of AMPA Receptor-TARP Complex by Cryo-EM. *Cell*, *170*(6), 1234-
674 1246 e1214. https://doi.org/10.1016/j.cell.2017.07.045
675 Cheng, X., Wang, H., Grant, B., Sine, S. M., & McCammon, J. A. (2006). Targeted molecular dynamics
676 study of C-loop closure and channel gating in nicotinic receptors. *PLoS Comput Biol*, *2*(9), e134.
677 https://doi.org/10.1371/journal.pcbi.0020134
678 Du, J., Lu, W., Wu, S., Cheng, Y., & Gouaux, E. (2015). Glycine receptor mechanism elucidated by electron
679 cryo-microscopy. *Nature*, *526*(7572), 224-229. https://doi.org/10.1038/nature14853
680 Furukawa, H., Singh, S. K., Mancusso, R., & Gouaux, E. (2005). Subunit arrangement and function in
681 NMDA receptors. *Nature*, *438*(7065), 185-192. https://doi.org/10.1038/nature04089
682 Gay, E. A., & Yakel, J. L. (2007). Gating of nicotinic ACh receptors; new insights into structural transitions
683 triggered by agonist binding that induce channel opening. *J Physiol*, *584*(Pt 3), 727-733.
684 https://doi.org/10.1113/jphysiol.2007.142554
685 Genheden, S., & Ryde, U. (2015). The MM/PBSA and MM/GBSA methods to estimate ligand-binding
686 affinities. *Expert Opin Drug Discov*, *10*(5), 449-461.
687 https://doi.org/10.1517/17460441.2015.1032936

Gharpure, A., Teng, J., Zhuang, Y., Noviello, C. M., Walsh, R. M., Jr., Cabuco, R., Howard, R. J., Zaveri, N. T., Lindahl, E., & Hibbs, R. E. (2019). Agonist Selectivity and Ion Permeation in the alpha3beta4 Ganglionic Nicotinic Receptor. *Neuron*, *104*(3), 501-511 e506. https://doi.org/10.1016/j.neuron.2019.07.030

Grosman, C., & Auerbach, A. (2001). The dissociation of acetylcholine from open nicotinic receptor channels. *Proc Natl Acad Sci U S A*, *98*(24), 14102-14107. https://doi.org/10.1073/pnas.251402498

Grosman, C., Zhou, M., & Auerbach, A. (2000). Mapping the conformational wave of acetylcholine receptor channel gating. *Nature*, *403*(6771), 773-776. https://doi.org/10.1038/35001586

Gupta, S., Chakraborty, S., Vij, R., & Auerbach, A. (2017). A mechanism for acetylcholine receptor gating based on structure, coupling, phi, and flip. *J Gen Physiol*, *149*(1), 85-103. https://doi.org/10.1085/jgp.201611673

Hansen, S. B., Sulzenbacher, G., Huxford, T., Marchot, P., Taylor, P., & Bourne, Y. (2005). Structures of Aplysia AChBP complexes with nicotinic agonists and antagonists reveal distinctive binding interfaces and conformations. *Embo Journal*, *24*(20), 3635-3646. https://doi.org/10.1038/sj.emboj.7600828

Hibbs, R. E., & Gouaux, E. (2011). Principles of activation and permeation in an anion-selective Cys-loop receptor. *Nature*, *474*(7349), 54-60. https://doi.org/10.1038/nature10139

Hibbs, R. E., Sulzenbacher, G., Shi, J., Talley, T. T., Conrod, S., Kem, W. R., Taylor, P., Marchot, P., & Bourne, Y. (2009). Structural determinants for interaction of partial agonists with acetylcholine binding protein and neuronal alpha7 nicotinic acetylcholine receptor. *Embo Journal*, *28*(19), 3040-3051. https://doi.org/10.1038/emboj.2009.227

Hou, T., Wang, J., Li, Y., & Wang, W. (2011). Assessing the performance of the MM/PBSA and MM/GBSA methods. 1. The accuracy of binding free energy calculations based on molecular dynamics simulations. *Journal of Chemical Information and Modeling*, *51*(1), 69-82. https://doi.org/10.1021/ci100275a

Huang, W., Manglik, A., Venkatakrishnan, A. J., Laeremans, T., Feinberg, E. N., Sanborn, A. L., Kato, H. E., Livingston, K. E., Thorsen, T. S., Kling, R. C., Granier, S., Gmeiner, P., Husbands, S. M., Traynor, J. R., Weis, W. I., Steyaert, J., Dror, R. O., & Kobilka, B. K. (2015). Structural insights into micro-opioid receptor activation. *Nature*, *524*(7565), 315-321. https://doi.org/10.1038/nature14886

Humphrey, W., Dalke, A., & Schulten, K. (1996). VMD: visual molecular dynamics. *J Mol Graph*, *14*(1), 33-38, 27-38. https://doi.org/10.1016/0263-7855(96)00018-5

Indurthi, D., & Auerbach, A. (2021). Agonist Efficiency Estimated from Concentration Response Curve. *Biophysical Journal*, *120*(3), 57a-57a. <Go to ISI>://WOS:000629601400276

Indurthi, D. C., & Auerbach, A. (2023). Agonist efficiency links binding and gating in a nicotinic receptor. *Elife*, *12*. https://doi.org/10.7554/eLife.86496

Jackson, M. B. (1986). Kinetics of unliganded acetylcholine receptor channel gating. *Biophys J*, *49*(3), 663-672. https://doi.org/10.1016/S0006-3495(86)83693-1

Jadey, S., & Auerbach, A. (2012). An integrated catch-and-hold mechanism activates nicotinic acetylcholine receptors. *J Gen Physiol*, *140*(1), 17-28. https://doi.org/10.1085/jgp.201210801

Klabunde, T., Petrassi, H. M., Oza, V. B., Raman, P., Kelly, J. W., & Sacchettini, J. C. (2000). Rational design of potent human transthyretin amyloid disease inhibitors. *Nat Struct Biol*, *7*(4), 312-321. https://doi.org/10.1038/74082

Klei, H. E., Kish, K., Lin, P. F., Guo, Q., Friborg, J., Rose, R. E., Zhang, Y., Goldfarb, V., Langley, D. R., Wittekind, M., & Sheriff, S. (2007). X-ray crystal structures of human immunodeficiency virus type 1 protease mutants complexed with atazanavir. *J Virol*, *81*(17), 9525-9535. https://doi.org/10.1128/JVI.02503-05

Kollman, P. A., Massova, I., Reyes, C., Kuhn, B., Huo, S., Chong, L., Lee, M., Lee, T., Duan, Y., Wang, W., Donini, O., Cieplak, P., Srinivasan, J., Case, D. A., & Cheatham, T. E., 3rd. (2000). Calculating structures and free energies of complex molecules: combining molecular mechanics and continuum models. *Acc Chem Res*, *33*(12), 889-897. https://doi.org/10.1021/ar000033j

Ma, W., Tang, C., & Lai, L. (2005). Specificity of trypsin and chymotrypsin: loop-motion-controlled dynamic correlation as a determinant. *Biophys J*, *89*(2), 1183-1193. https://doi.org/10.1529/biophysj.104.057158

Mittal, L., Srivastava, M., Kumari, A., Tonk, R. K., Awasthi, A., & Asthana, S. (2021). Interplay among Structural Stability, Plasticity, and Energetics Determined by Conformational Attuning of Flexible Loops in PD-1. *Journal of Chemical Information and Modeling*, *61*(1), 358-384. https://doi.org/10.1021/acs.jcim.0c01080

Mittal, L., Tonk, R. K., Awasthi, A., & Asthana, S. (2021). Targeting cryptic-orthosteric site of PD-L1 for inhibitor identification using structure-guided approach. *Arch Biochem Biophys*, *713*, 109059. https://doi.org/10.1016/j.abb.2021.109059

Mukhtasimova, N., Free, C., & Sine, S. M. (2005). Initial coupling of binding to gating mediated by conserved residues in the muscle nicotinic receptor. *J Gen Physiol*, *126*(1), 23-39. https://doi.org/10.1085/jgp.200509283

Munro, L., Ladefoged, L. K., Padmanathan, V., Andersen, S., Schiott, B., & Kristensen, A. S. (2019). Conformational Changes in the 5-HT(3A) Receptor Extracellular Domain Measured by Voltage-Clamp Fluorometry. *Molecular Pharmacology*, *96*(6), 720-734. https://doi.org/10.1124/mol.119.116657

Muroi, Y., Theusch, C. M., Czajkowski, C., & Jackson, M. B. (2009). Distinct structural changes in the GABAA receptor elicited by pentobarbital and GABA. *Biophys J*, *96*(2), 499-509. https://doi.org/10.1016/j.bpj.2008.09.037

Nayak, T. K., & Auerbach, A. (2017). Cyclic activation of endplate acetylcholine receptors. *Proc Natl Acad Sci U S A*, *114*(45), 11914-11919. https://doi.org/10.1073/pnas.1711228114

Nayak, T. K., Chakraborty, S., Zheng, W. J., & Auerbach, A. (2016). Structural correlates of affinity in fetal versus adult endplate nicotinic receptors. *Nature Communications*, *7*. https://doi.org/ARTN 11352

10.1038/ncomms11352

Nayak, T. K., Purohit, P. G., & Auerbach, A. (2012). The intrinsic energy of the gating isomerization of a neuromuscular acetylcholine receptor channel. *J Gen Physiol*, *139*(5), 349-358. https://doi.org/10.1085/jgp.201110752

Nayak, T. K., Vij, R., Bruhova, I., Shandilya, J., & Auerbach, A. (2019). Efficiency measures the conversion of agonist binding energy into receptor conformational change. *J Gen Physiol*, *151*(4), 465-477. https://doi.org/10.1085/jgp.201812215

Nickbarg, E. B., Davenport, R. C., Petsko, G. A., & Knowles, J. R. (1988). Triosephosphate isomerase: removal of a putatively electrophilic histidine residue results in a subtle change in catalytic mechanism. *Biochemistry*, *27*(16), 5948-5960. https://doi.org/10.1021/bi00416a019

Noviello, C. M., Gharpure, A., Mukhtasimova, N., Cabuco, R., Baxter, L., Borek, D., Sine, S. M., & Hibbs, R. E. (2021). Structure and gating mechanism of the alpha7 nicotinic acetylcholine receptor. *Cell*, *184*(8), 2121-2134 e2113. https://doi.org/10.1016/j.cell.2021.02.049

Oostenbrink, C., Villa, A., Mark, A. E., & van Gunsteren, W. F. (2004). A biomolecular force field based on the free enthalpy of hydration and solvation: the GROMOS force-field parameter sets 53A5 and 53A6. *J Comput Chem*, *25*(13), 1656-1676. https://doi.org/10.1002/jcc.20090

Padgett, C. L., Hanek, A. P., Lester, H. A., Dougherty, D. A., & Lummis, S. C. (2007). Unnatural amino acid mutagenesis of the GABA(A) receptor binding site residues reveals a novel cation-pi interaction

between GABA and beta 2Tyr97. *Journal of Neuroscience*, *27*(4), 886-892. https://doi.org/10.1523/JNEUROSCI.4791-06.2007

Pettersen, E. F., Goddard, T. D., Huang, C. C., Meng, E. C., Couch, G. S., Croll, T. I., Morris, J. H., & Ferrin, T. E. (2021). UCSF ChimeraX: Structure visualization for researchers, educators, and developers. *Protein Sci*, *30*(1), 70-82. https://doi.org/10.1002/pro.3943

Plapp, B. V. (2010). Conformational changes and catalysis by alcohol dehydrogenase. *Arch Biochem Biophys*, *493*(1), 3-12. https://doi.org/10.1016/j.abb.2009.07.001

Pless, S. A., Hanek, A. P., Price, K. L., Lynch, J. W., Lester, H. A., Dougherty, D. A., & Lummis, S. C. (2011). A cation-pi interaction at a phenylalanine residue in the glycine receptor binding site is conserved for different agonists. *Molecular Pharmacology*, *79*(4), 742-748. https://doi.org/10.1124/mol.110.069583

Pless, S. A., & Lynch, J. W. (2009). Ligand-specific conformational changes in the alpha1 glycine receptor ligand-binding domain. *J Biol Chem*, *284*(23), 15847-15856. https://doi.org/10.1074/jbc.M809343200

Polovinkin, L., Hassaine, G., Perot, J., Neumann, E., Jensen, A. A., Lefebvre, S. N., Corringer, P. J., Neyton, J., Chipot, C., Dehez, F., Schoehn, G., & Nury, H. (2018). Conformational transitions of the serotonin 5-HT(3) receptor. *Nature*, *563*(7730), 275-279. https://doi.org/10.1038/s41586-018-0672-3

Purohit, P., & Auerbach, A. (2009). Unliganded gating of acetylcholine receptor channels. *Proc Natl Acad Sci U S A*, *106*(1), 115-120. https://doi.org/10.1073/pnas.0809272106

Purohit, P., & Auerbach, A. (2013). Loop C and the mechanism of acetylcholine receptor-channel gating. *J Gen Physiol*, *141*(4), 467-478. https://doi.org/10.1085/jgp.201210946

Purohit, P., Bruhova, I., Gupta, S., & Auerbach, A. (2014). Catch-and-Hold Activation of Muscle Acetylcholine Receptors Having Transmitter Binding Site Mutations. *Biophysical Journal*, *107*(1), 88-99. https://doi.org/10.1016/j.bpj.2014.04.057

Purohit, P., Gupta, S., Jadey, S., & Auerbach, A. (2013). Functional anatomy of an allosteric protein. *Nature Communications*, *4*, 2984. https://doi.org/10.1038/ncomms3984

Purushotham, N., Singh, M., Paramesha, B., Kumar, V., Wakode, S., Banerjee, S. K., Poojary, B., & Asthana, S. (2022). Design and synthesis of amino acid derivatives of substituted benzimidazoles and pyrazoles as Sirt1 inhibitors. *RSC Adv*, *12*(7), 3809-3827. https://doi.org/10.1039/d1ra06149f

Rahman, M. M., Basta, T., Teng, J., Lee, M., Worrell, B. T., Stowell, M. H. B., & Hibbs, R. E. (2022). Structural mechanism of muscle nicotinic receptor desensitization and block by curare. *Nat Struct Mol Biol*, *29*(4), 386-394. https://doi.org/10.1038/s41594-022-00737-3

Rahman, M. M., Teng, J., Worrell, B. T., Noviello, C. M., Lee, M., Karlin, A., Stowell, M. H. B., & Hibbs, R. E. (2020). Structure of the Native Muscle-type Nicotinic Receptor and Inhibition by Snake Venom Toxins. *Neuron*, *106*(6), 952-962 e955. https://doi.org/10.1016/j.neuron.2020.03.012

Rasmussen, S. G., DeVree, B. T., Zou, Y., Kruse, A. C., Chung, K. Y., Kobilka, T. S., Thian, F. S., Chae, P. S., Pardon, E., Calinski, D., Mathiesen, J. M., Shah, S. T., Lyons, J. A., Caffrey, M., Gellman, S. H., Steyaert, J., Skiniotis, G., Weis, W. I., Sunahara, R. K., & Kobilka, B. K. (2011). Crystal structure of the beta2 adrenergic receptor-Gs protein complex. *Nature*, *477*(7366), 549-555. https://doi.org/10.1038/nature10361

Rastelli, G., Del Rio, A., Degliesposti, G., & Sgobba, M. (2010). Fast and accurate predictions of binding free energies using MM-PBSA and MM-GBSA. *J Comput Chem*, *31*(4), 797-810. https://doi.org/10.1002/jcc.21372

Roe, D. R., & Cheatham, T. E., 3rd. (2013). PTRAJ and CPPTRAJ: Software for Processing and Analysis of Molecular Dynamics Trajectory Data. *J Chem Theory Comput*, *9*(7), 3084-3095. https://doi.org/10.1021/ct400341p

Shang, Y., Yeatman, H. R., Provasi, D., Alt, A., Christopoulos, A., Canals, M., & Filizola, M. (2016). Proposed Mode of Binding and Action of Positive Allosteric Modulators at Opioid Receptors. *ACS Chem Biol*, *11*(5), 1220-1229. https://doi.org/10.1021/acschembio.5b00712

Sigel, E., & Steinmann, M. E. (2012). Structure, function, and modulation of GABA(A) receptors. *J Biol Chem*, *287*(48), 40224-40231. https://doi.org/10.1074/jbc.R112.386664

Singh, M., Srivastava, M., Wakode, S. R., & Asthana, S. (2021). Elucidation of Structural Determinants Delineates the Residues Playing Key Roles in Differential Dynamics and Selective Inhibition of Sirt1-3. *Journal of Chemical Information and Modeling*, *61*(3), 1105-1124. https://doi.org/10.1021/acs.jcim.0c01193

Srivastava, M., Mittal, L., Kumari, A., Agrahari, A. K., Singh, M., Mathur, R., & Asthana, S. (2022). Characterizing (un)binding mechanism of USP7 inhibitors to unravel the cause of enhanced binding potencies at allosteric checkpoint. *Protein Sci*, *31*(9), e4398. https://doi.org/10.1002/pro.4398

Sun, H., Li, Y., Tian, S., Xu, L., & Hou, T. (2014). Assessing the performance of MM/PBSA and MM/GBSA methods. 4. Accuracies of MM/PBSA and MM/GBSA methodologies evaluated by various simulation protocols using PDBbind data set. *Phys Chem Chem Phys*, *16*(31), 16719-16729. https://doi.org/10.1039/c4cp01388c

Tarvin, R. D., Borghese, C. M., Sachs, W., Santos, J. C., Lu, Y., O'Connell, L. A., Cannatella, D. C., Harris, R. A., & Zakon, H. H. (2017). Interacting amino acid replacements allow poison frogs to evolve epibatidine resistance. *Science*, *357*(6357), 1261-1266. https://doi.org/10.1126/science.aan5061

Tian, C., Kasavajhala, K., Belfon, K. A. A., Raguette, L., Huang, H., Migues, A. N., Bickel, J., Wang, Y., Pincay, J., Wu, Q., & Simmerling, C. (2020). ff19SB: Amino-Acid-Specific Protein Backbone Parameters Trained against Quantum Mechanics Energy Surfaces in Solution. *J Chem Theory Comput*, *16*(1), 528-552. https://doi.org/10.1021/acs.jctc.9b00591

Tripathy, S., Zheng, W., & Auerbach, A. (2019). A single molecular distance predicts agonist binding energy in nicotinic receptors. *J Gen Physiol*, *151*(4), 452-464. https://doi.org/10.1085/jgp.201812212

Unwin, N. (1993). Nicotinic acetylcholine receptor at 9 A resolution. *J Mol Biol*, *229*(4), 1101-1124. https://doi.org/10.1006/jmbi.1993.1107

Vassetti, D., Pagliai, M., & Procacci, P. (2019). Assessment of GAFF2 and OPLS-AA General Force Fields in Combination with the Water Models TIP3P, SPCE, and OPC3 for the Solvation Free Energy of Druglike Organic Molecules. *J Chem Theory Comput*, *15*(3), 1983-1995. https://doi.org/10.1021/acs.jctc.8b01039

Wagner, J. R., Sorensen, J., Hensley, N., Wong, C., Zhu, C., Perison, T., & Amaro, R. E. (2017). POVME 3.0: Software for Mapping Binding Pocket Flexibility. *J Chem Theory Comput*, *13*(9), 4584-4592. https://doi.org/10.1021/acs.jctc.7b00500

Walsh, R. M., Jr., Roh, S. H., Gharpure, A., Morales-Perez, C. L., Teng, J., & Hibbs, R. E. (2018). Structural principles of distinct assemblies of the human alpha4beta2 nicotinic receptor. *Nature*, *557*(7704), 261-265. https://doi.org/10.1038/s41586-018-0081-7

Wlodawer, A., & Erickson, J. W. (1993). Structure-based inhibitors of HIV-1 protease. *Annu Rev Biochem*, *62*, 543-585. https://doi.org/10.1146/annurev.bi.62.070193.002551

Xiu, X., Puskar, N. L., Shanata, J. A., Lester, H. A., & Dougherty, D. A. (2009). Nicotine binding to brain receptors requires a strong cation-pi interaction. *Nature*, *458*(7237), 534-537. https://doi.org/10.1038/nature07768

Zarkadas, E., Pebay-Peyroula, E., Thompson, M. J., Schoehn, G., Uchanski, T., Steyaert, J., Chipot, C., Dehez, F., Baenziger, J. E., & Nury, H. (2022). Conformational transitions and ligand-binding to a muscle-type nicotinic acetylcholine receptor. *Neuron*, *110*(8), 1358-1370 e1355. https://doi.org/10.1016/j.neuron.2022.01.013

Zhong, W., Gallivan, J. P., Zhang, Y., Li, L., Lester, H. A., & Dougherty, D. A. (1998). From ab initio quantum mechanics to molecular neurobiology: a cation-pi binding site in the nicotinic receptor. *Proc Natl Acad Sci U S A*, *95*(21), 12088-12093. https://doi.org/10.1073/pnas.95.21.12088